# Novel Multicode-Processing Platform for Wavelength-Hopping Time-Spreading Optical CDMA: A Path to Device Miniaturization and Enhanced Network Functionality

Yue-Kai Huang, *Student Member, IEEE*, Varghese Baby, *Student Member, IEEE*, Ivan Glesk, *Senior Member, IEEE*, Camille-Sophie Bres, *Student Member, IEEE*, Christoph M. Greiner, *Member, IEEE*, Dmitri Iazikov, *Member, IEEE*, Thomas W. Mossberg, *Member, IEEE*, and Paul R. Prucnal, *Fellow, IEEE*

***Abstract*—Cost-effective, robust, code-processing photonic devices are essential for the adoption of optical code-division multiple access in future commercial and military network applications. Progress in several technology platforms for code processing is summarized. In particular, we focus on developments in a technology platform based on holographic Bragg reflectors that allow the processing of multiple codes simultaneously, with low footprint. Results of simultaneous en/decoding of two wavelength-hopping time-spreading codes using a single device are presented. Several applications are presented where multicode-processing capability can result in significant simplification of node and system architectures and, thus, provide feasible implementation of schemes to obtain enhanced network performance such as security and scalability.**

***Index Terms*—Coder–decoders, holographic Bragg reflector (HBR), integrated photonic circuit, optical code-division multiple access (OCDMA), security.**

## I. Introduction

INCOHERENT optical code-division multiple access (OCDMA) has recently attracted wide attention due to its robust performance, phase insensitivity, asynchronous network access capability, and flexible bandwidth provisioning [1]. OCDMA is, thus, envisioned as a technology that can easily provide the bandwidth demands of future fiber-to-the-home (FTTH) services [2]. Wavelength-hopping time-spreading (WHTS), a 2-D incoherent OCDMA approach that spreads the codes in both the time and wavelength domains simultaneously [3], provides several advantages over other incoherent OCDMA schemes such as increased code-design flexibility and code performance. We had previously demonstrated two WHTS testbeds with commercial-off-the- shelf (COTS) technologies using simple on/off key data modulation [4] and using $M$-ary data modulation as a means for scaling to higher number of users and improved performance [5]. However, practical system implementations, both in commercial and military networks, will require that code-processing devices (e.g., encoders and decoders at the transmitter and receiver end, respectively) be made using robust, lightweight, and low-cost technology platforms. Various technology platforms have been used in the past for achieving code processing in WHTS OCDMA. Here, we summarize the different choices before primarily focusing on a relatively new technology platform based on holographic Bragg reflector (HBR). A key feature of the technology is that multiple codes can be processed simultaneously using a single device. We will experimentally study this capability using a device that can process two codes simultaneously. We will also evaluate the benefits of multicode-processing devices on the design of OCDMA networks and provide several applications where multicode processing can result in significant benefits.

This paper is divided into several sections. The general principles of WHTS OCDMA networks are outlined in Section II. Various device technologies for WHTS code processing are summarized in Section III. Section IV presents the HBR technology along with the results of dual-code WHTS encoding using an HBR-based device. Section V focuses on various applications of multicode-processing devices in an OCDMA network for enhanced network performance. Applications include schemes for enhanced security, enhanced network scalability, simplified low-cost node architectures, and low-cost OCDMA network monitoring. Section VI summarizes the conclusions and discussions.

## II. WHTS System

As mentioned in Section I, WHTS system is a 2-D optical coding approach that spreads the codes in both time and wavelength domains, simultaneously [3]. Low cross correlations and higher cardinality can be obtained at reduced code lengths compared to 1-D temporal OCDMA, allowing for improved network performance. In addition, zero autocorrelation side-lobes obtained in WHTS systems allow easy synchronization between the transmitter and the intended receiver. In WHTS, code sequences are created by placing pulses of different wavelengths in different time chips by following a hopping pattern prescribed by the used

Manuscript received December 18, 2006; revised March 15, 2007. This work was supported in part by the Defense Advanced Research Projects Agency, in part by the Photonics Technology Access Program, and in part by Lockheed Martin.

Y.-K. Huang, I. Glesk, C.-S. Bres, and P. R. Prucnal are with the Department of Electrical Engineering, Princeton University, Princeton, NJ 08540 USA (e-mail: yuehuang@princeton.edu; glesk@princeton.edu; cbres@princeton.edu; prucnal@princeton.edu).

V. Baby was with the Department of Electrical Engineering, Princeton University, Princeton, NJ 08540 USA. He is currently with the Department of Electrical and Computer Engineering, McGill University, Montreal, QC H3A 2T5, Canada (e-mail: varghese.baby@mail.mcgill.ca).

C. M. Greiner, D. Iazikov, and T. W. Mossberg are with LightSmyth Technologies, Inc., Eugene, OR 97402 USA (e-mail: cgreiner@lightsmyth.com; diazikov@lightsmyth.com; twmoss@lightsmyth.com).

Digital Object Identifier 10.1109/JSTQE.2007.896098

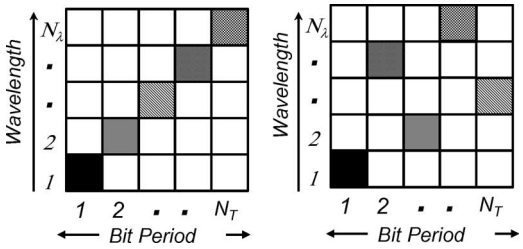


Fig. 1. Two code sequences for WHTS OCDMA. The bit period is divided into $N_T$ chips ($N_T$: code length), and code sequences are formed by placing $w$ ($w$: code weight) pulses of different wavelengths ($N_\lambda$: number of different wavelengths) in them.

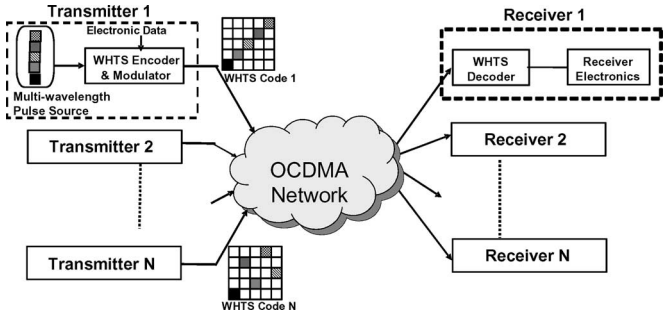


Fig. 2. Schematic of a general WHTS OCDMA network.

code sequence [6]. Thus, WHTS codes can be represented as 2-D code matrices in time and wavelength dimensions. The wavelength domain is divided into $N_\lambda$ wavelength channels, and the time domain is divided into $N_T$ chips. The 2-D representation of two code sequences is given in Fig. 1. A total number of $w$ pulses ($w$ : code weight) are positioned within the matrix [6].

All active users share the same code space created from available wavelengths and time domain, thus, providing a fair division of the bandwidth. This is in contrast to the other multiplexing/multiple access approaches such as optical time-division multiplexing (OTDM) and wavelength-division multiplexing (WDM) where only a small portion of the bandwidth is allocated to each user. While OTDM requires strict synchronization between users, WHTS OCDMA provides truly asynchronous access that greatly simplifies network control and management. Both WDM- and TDM-based schemes are limited in scalability of the number of users by the number of available wavelengths and the number of time slots, respectively. On the other hand, the number of users in a WHTS OCDMA network has a soft limit with a graceful degradation of performance as the number of users increases. Differentiated service can be provisioned in the physical layer in WHTS by varying the code weight that is assigned to each user, as shown in our recent demonstration [7]. Thus, performance can be easily changed to accommodate different classes of service based on user demands. Code properties also allow the coexistence of users with different data rates [8]. The ability of WHTS to handle differentiated service and multiple data rates will be of key benefit to next generation access networks [9].

A general schematic of a WHTS OCDMA network is shown in Fig. 2. Most OCDMA demonstrations have used a broadcast star topology [9], [10], though other topologies such as ring and bus have also been considered [11], [12]. The two main elements of the transmitter are the optical source and the OCDMA encoder. The receiver consists of the OCDMA decoder followed by the receiver electronics. The optical source can be implemented using multiwavelength laser made either by using an array of lasers each operating at a fixed wavelength, a single laser lasing at multiple wavelengths [13], or by spectral slicing a broadband optical spectrum from a supercontinuum source [14] or semiconductor laser diode [15]. The multiwavelength output is fed into the optical encoder, which forms the WHTS code sequence. Data modulation is done either before or after the encoding, depending on the transmitter design and network application.

The WHTS encoder selects $w$ pulses of $N_\lambda$ wavelengths and positions them within $N_T$ chips of the bit interval as prescribed by the code sequence. Thus, the encoder essentially performs two processes: wavelength hopping and time spreading. WHTS encoders have been implemented using different technologies. Demonstrations have shown the use of arrayed waveguide gratings (AWGs) or thin-film filters (TFFs) for the control of the wavelength-hopping processing, while fixed or tunable delay lines have been used to control the time-spreading process [16], [17]. On the other hand, encoders/decoders based on chirped Moire gratings (CMGs) and HBRs efficiently combine wavelength hopping and time spreading into a single process, resulting in reduction of the WHTS encoder/decoder footprint.

In broadcast networks, the signals from all the transmitters are received by the WHTS receiver. In a fixed receiver addressing scheme, the optical decoder discriminates between the intended and interfering data streams by correlating the received signal with the code sequence assigned to that receiver. In the case of a matched signal, this process will undo the time spreading, aligning the wavelength pulses back in time on top of each other to form an autocorrelation peak of height $w$ ($w$ : code weight). For the other received code sequences, as the optical decoder is not matched to them, the different wavelength pulses are further spread over the bit period resulting in low-intensity multiple-access interference (MAI).

The structure of the WHTS decoder is, thus, very similar to that of a WHTS encoder; wavelength-dependant delay element operates over the entire signal bandwidth. This device architecture is used not only for WHTS en/decoders but also for other functional elements such as code restorers in OCDMA ring networks [10], [18], code converters in a code-based OCDMA router [11], etc. Our next sections will focus on the technology platforms for this type of WHTS code-processing devices.

## III. Platforms for Code Processing

### A. TFFs

Thin-film optics has been studied for a variety of applications including edge filters, antireflection coatings, and high-reflectance coatings [19]. A TFF is essentially an Fabry–Perot etalon with reflective "mirrors" formed using dielectric thin films. Thus, a TFF acts as a bandpass filter. In an extension of this idea, thin-film resonant multicavity filters have been built by having two or more cavities separated by reflective dielectric thin-film layers. By varying the number of cavities, different

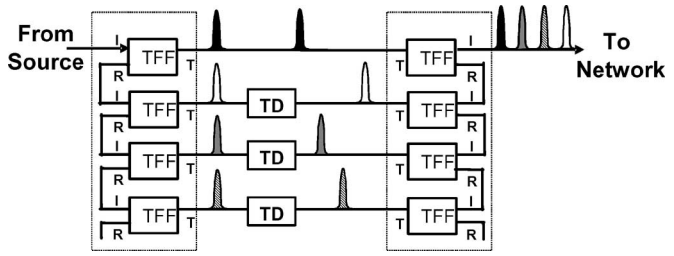


Fig. 3. Schematic of a WHTS encoder with four wavelengths in the code and using TFFs (I: input port; T: transmitted port; R: reflected port) technologies.

features of the transmission spectral profile such as the shape of the pass band and the steepness of its falling and rising edges can be varied.

Wavelength multiplexers and demultiplexers can be formed by cascading a number of TFFs. Fig. 3 shows the use of a TFF-based multiplexer and demultiplexer to form a WHTS encoder. Tunable TFFs have been demonstrated using different mechanisms such as current injection techniques in InGaAsP/InP waveguides, and change of optical thickness using piezo-electric effect and thermo-optic effect [20]–[24].

TFFs have emerged as a dominant filter technology in commercial markets due to their flexibility, low loss, and passive temperature compensation. They provide the lowest-loss solution at low channel count, and similar loss to flat-top arrayed-waveguide gratings at high channel counts. In addition, the device is insensitive to the polarization of the signal and extremely stable to temperature variations. TFFs have been used for various optical networking applications such as switchable add–drop filters [24] and optical switches [25].

TFFs have been used in WHTS en/decoders in some recent WHTS demonstrations [4], [5]. The minimal chip size in these networks is limited by pulse broadening due to propagation through dispersive TFFs. While TFF-based solution provides excellent passband characteristics for spectral slicing, additional external delay lines needed to construct WHTS en/decoders make these devices harder to integrate in one device.

### *B. FBGs*

FBGs have been used for various applications in optical networks such as add–drop multiplexing and wavelength routing in WDM networks, dispersion compensation, and wavelength stabilization techniques in fiber lasers [26], [27]. FBGs have also been used to implement various OCDMA encoding schemes such as spectral-amplitude coding [28], temporal-phase coding [29], and spectral-phase coding [30]. A super-structured FBG was used to generate a 511-chip phase-shift keyed code with 10-nm spectral width [2]. FBGs provide a simple and elegant all-fiber approach with tunability achieved using both strain and temperature effects [27].

Implementation of WHTS using FBGs have been done using two structures: linear array of FBGs and CMGs. Fig. 4(a) shows the implementation of a WHTS code using a linear array of FBGs [31]. As a generalization of this structure, parallel linear arrays can be used with a power divider to implement multiple pulses per column (MPPC) codes [32] (i.e., multiple wavelengths occupying the same chip), as shown in Fig. 4(b).

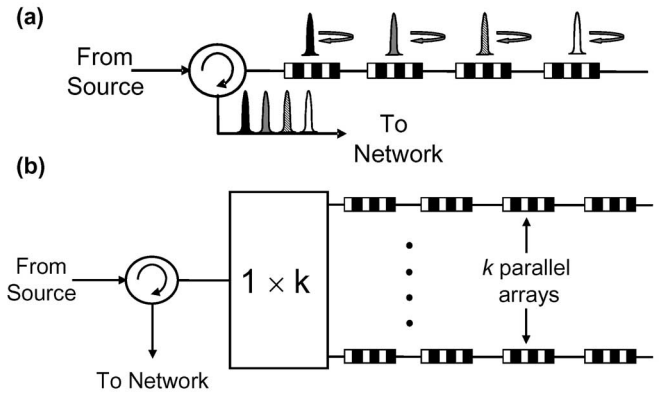


Fig. 4. (a) Schematic of a WHTS encoder with four wavelengths in the code and using a linear array of FBG. (b) Parallel linear array of FBGs allows implementation of MPPC codes. $k$ is the maximum number of wavelengths in the same column of the code matrix [32].

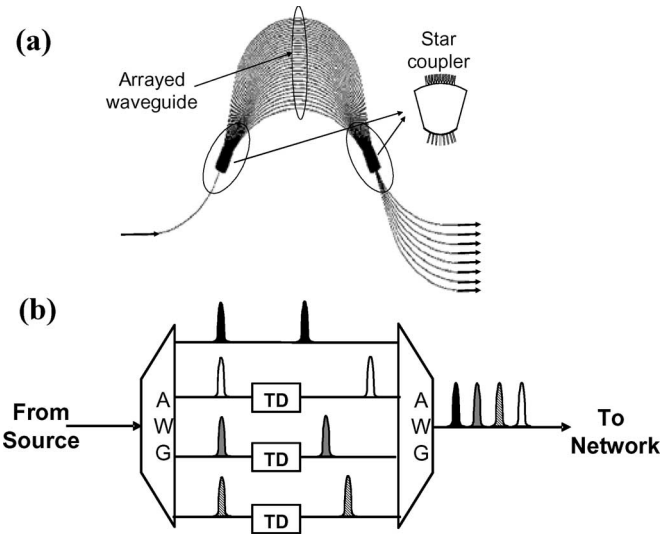


Fig. 5. Schematic of (a) an AWG [34] and (b) a WHTS encoder with four wavelengths in the code using AWG technologies.

CMGs that are composed of superposed linearly chirped FBGs enable the use of a single passive grating structure to implement WHTS en/decoding [33]. However, the linear relationship between wavelengths and time, which results in an inherent coupling of the wavelength-hopping and time-spreading patterns in CMGs, restricts the types and numbers of codes that can be implemented using this structure.

The chip size in FBG-based WHTS en/decoders is limited by the minimum possible spacing between adjacent gratings [31]. In addition, additional components such as power splitters or circulators are needed for the separation of coded/decoded signals resulting in increased system complexity and cost.

### *C. AWGs*

Since the early 90s, AWG has been another widely researched technology platform due to its potential for low insertion loss [34]. As shown in Fig. 5(a), it consists of a phased array of optical waveguides that acts as a grating. The input signal is coupled into an array of planar waveguides after passing through a free-propagation region. The waveguides are designed to be

of different lengths to provide different phase shifts to the signal in each waveguide. Also, these phase shifts are wavelength dependent because of the frequency dependence of the mode-propagation constant. As a result, different wavelength channels focus to different output waveguides when the light exiting from the array diffracts in another free-propagation region. The input and output waveguides, the multiport couplers, and the arrayed waveguides are all fabricated on a single substrate.

AWGs have been used in various applications such as wavelength multiplexers or demultiplexers, $N \times N$ wavelength routers [35], optical cross connects [36], WDM transmitters to supply multiwavelengths [37], [38], and integrated WDM receivers to provide routing to photodiode array [39]. AWGs with more than 100 ports have been reported [40], while devices with more than 50 ports are commercially available.

Fig. 5(b) shows a simple implementation of a WHTS en/decoder using two AWGs: 1) a $1 \times N$ wavelength demultiplexer and 2) a $N \times 1$ wavelength multiplexer with fixed or tunable delay lines in between. En/decoding using a single AWG was also demonstrated in a feedback configuration with fiber loops for delays [14] utilizing the bidirectional nature of the AWGs. A fold-back configuration with mirrored fiber delay lines was used for performing both encoding and decoding with a single AWG [41]. In a recent waveguide-grating-router (WGR) configuration, a full set of orthogonal codes was generated using a pair of AWGs by multipath slab reflection effect [42]. An AWG can be integrated together with the waveguide-based delays to form a complete WHTS optical en/decoder.

## IV. HBRs

HBRs [43] are computer-generated planar volume holograms fabricated in slab waveguides using deep UV photolithography. Like TFFs, HBR-based filtering relies on multipath interference. The HBR technology, thus, transfers the excellent passband control associated with TFFs with the planar lightwave circuit environment. Integrated-circuit fabrication technology and, to even larger degree, embossing-based replication methods will ultimately provide very inexpensive devices in high volumes. The possibility of overlaying, stacking, and interleaving of individual HBRs [43] provides a pathway to build WHTS en/decoders for simultaneous multicode processing, with the potential to store a complete set of user code words in one device. In addition, the HBR-approach allows the simultaneous implementation of both spectral slicing and wavelength- dependant delay, resulting in a device footprint that can be an order of magnitude smaller than other approaches.

We have already presented the results showing the feasibility of the HBR-based device for WHTS en/decoding [44]. In this section, we will show the results of simultaneous processing of two WHTS codes using a single HBR-based device.

### A. Device Design and Fabrication

The HBR-based encoders and decoders were designed to fit an existing incoherent OCDMA four-user testbed [12] at OC-24 data rate that uses WHTS codes with three wavelengths and 11 time chips. The chip size was 73.1 ps and was limited only by

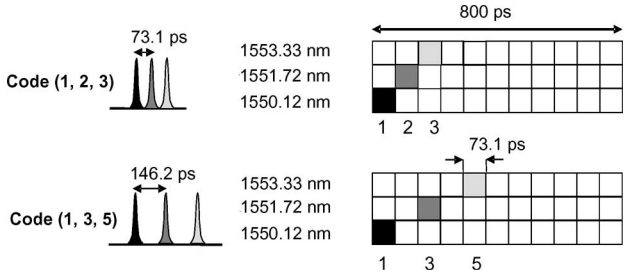


Fig. 6. (3, 11) WHTS code matrix and (1, 2, 3) and (1, 3, 5) codes.

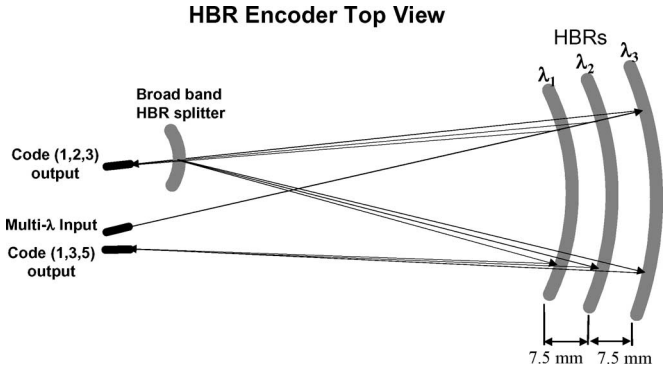


Fig. 7. Schematic top view of the $1 \times 2$ integrated holographic OCDMA encoder. The optical path for generation of code (1, 2, 3) is shown. A broadband HBR splits off a fraction of the exiting (1, 2, 3) code sequence and converts it to code (1, 3, 5) by double passing of the HBR array. Dimensions in the figure are not to scale.

the low-speed electronics used after the WHTS decoder. Carrier-hopping prime codes [6] were used for this demonstration. The three wavelengths were 1550.12 nm ($\lambda_1$), 1551.72 nm ($\lambda_2$), and 1553.33 nm ($\lambda_3$). The HBR-based encoder was designed to simultaneously produce two WHTS codes (1, 2, 3) and (1, 3, 5), where the numbers in parenthesis are the time chips in which $\lambda_1$, $\lambda_2$, and $\lambda_3$ were, respectively, placed. Fig. 6 shows the code matrix representation of the two designed codes.

Fig. 7 is a top-view schematic of the $1 \times 2$ HBR WHTS encoder. A pulse train with spectral width encompassing wavelengths $\lambda_1$ through $\lambda_3$ is inputted to the encoder through a channel waveguide from which it expands into a slab waveguide region. The latter contains three 5-mm-long HBR gratings, which select spectral slices centered at the desired wavelengths $\lambda_1$, $\lambda_2$, and $\lambda_3$. The gratings time delay the spectral selections by the amounts required to create WHTS code (1, 2, 3) at the output port 1 by virtue of their $\sim$7.5-mm center-to-center spacing along the input direction. The code sequence (1, 2, 3) thus created leaves the coder through output channel waveguide 1. A fourth 500-$\mu$m-long HBR, whose reflection passband encompasses all the three wavelengths, is located in front of output channel waveguide 1. A fraction of the impinging (1, 2, 3) code is split off and redirected back to the array of HBRs. As the split-off code (1, 2, 3) pulse sequence passes the HBR array for the second time, the time delays between the three spectral slices are doubled, creating the (1, 3, 5) code that exits the encoder through output 2. Double passing of the HBR array was only necessitated by the large time delay of 350 ps between $\lambda_1$ and $\lambda_3$ in the (1, 3, 5) code, which was not attainable in a single pass even by placing the $\lambda_1$ and $\lambda_3$ HBRs at opposite edges of

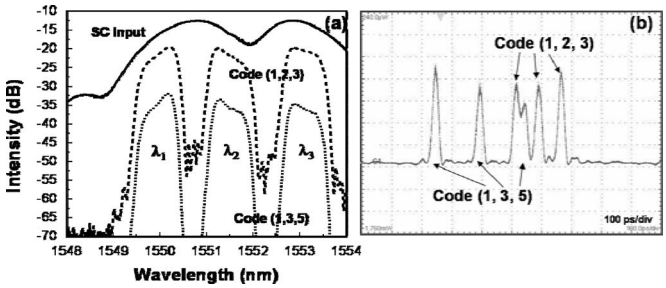


Fig. 8. (a) Spectra and (b) time signatures of the generated WHTS codes.

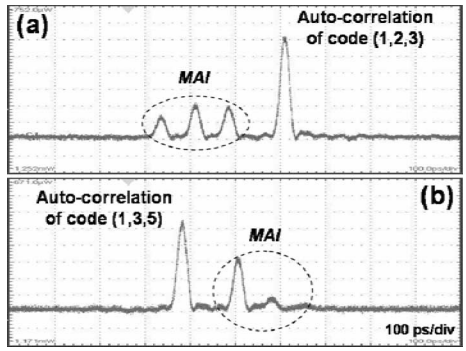


Fig. 9. The decoded autocorrelation peaks for (a) code (1, 2, 3) and (b) code (1, 3, 5) and cross-correlation signals arising from the nonmatching input.

the 33-mm-long die. Simple single-pass HBR-based en/decoder designs will be sufficient for the higher data rates (OC-48 and above) expected in future networks.

It is interesting to note that the double passing scheme of Fig. 7 uniquely leverages the similarity between the two codes whose difference lies in the intrachip time delays. This encoder design minimizes the number of HBRs required to generate the two code sequences and, thus, makes it possible to build a very compact device. In general, two arbitrary code sequences can be implemented in a coder if one HBR is employed per time/wavelength chip in a given code. The layout of the matched $1 \times 2$ HBR-based decoder (not shown) is identical to the encoder design of Fig. 7, except that the spatial positioning of the gratings occurs in opposite order (but with same relative distances) to correctly reverse the time delays created by the encoder. The HBR-based device employs a dual-layer core architecture [43] based on the silica-on-silicon platform. In the grating region, the high-index grating layer is 300-nm thick with diffractive contours of equal thickness, while the upper core layer is about 2.7-$\mu$m thick. Outside the grating regions, only a single core layer with index contrast of $\sim$0.7% to the claddings and thickness of 2.9 $\mu$m remains. Both encoder and decoder were fabricated from a laser-written reticle employing a deep UV optical stepper, standard etching, deposition, and annealing processes. The fabricated chips were pigtailed and packaged. The overall die size containing both encoder and decoder was only $5 \times 33$ mm$^2$.

### *B. Experimental Encoding and Decoding Performance*

The experimental generation of the WHTS OCDMA codes is done by injecting a 10-nm-wide 0.3-ps-long supercontinuum optical pulse into the HBR encoder. The supercontinuum pulse was generated by passing the amplified output of a 1550-nm mode-locked erbium-doped fiber laser through a piece of dispersion decreasing fiber. The optical spectrum of the two codes, as measured by an optical spectrum analyzer (resolution 0.1 nm), is depicted in Fig. 8(a), clearly showing the three spectral bins centered at the design wavelengths. The difference between output spectral powers for the two codes is due to the weak reflecting nature of the broadband HBR and can be easily rectified in future design. In the experiment, we used a tunable optical amplifier for code (1, 3, 5) to match the power level of code (1, 2, 3). The shape of the spectral bins and their relative intensity is slightly distorted due to the nonuniformity of the supercontinuum spectral intensity (shown as upper solid black line for reference). Note the excellent fall-off characteristics and spectral isolation of the spectral bins, achieved by apodizing the HBR using a correlated-line approach and a Gaussian-weighted sinc function [45].

In Fig. 8(b), we show the multiplexed temporal signatures of output ports 1 and 2 as detected with a bandwidth-limited optical sampling oscilloscope (30-GHz bandwidth). As clearly shown, both generated WHTS codes are in perfect agreement with the code designs regarding the temporal separation of the spectral chips, i.e., the $\lambda_1$, $\lambda_2$, and $\lambda_3$ pulses are $\sim$73 ps apart for code (1, 2, 3) and $\sim$146 ps apart for code (1, 3, 5). The intensity drop observed across the (1, 3, 5) pulse sequence is attributed to a grating-mediated out-coupling of waveguide signals to cladding and free-space modes. This loss mechanism scales with the aggregate grating length, both resonant and nonresonant, through which signals travel. The loss, therefore, gets worse for signals reflected from HBRs at the back of the encoder, i.e., for $\lambda_2$ and $\lambda_3$ pulses. This signal loss is partially compensated by the decoder where the $\lambda_1$ pulse experiences the largest loss. However, its effect on the MAI will still be present and, hence, needs to be reduced. This loss is specific to the particular apodization approach used in obtaining the spectral bin transfer functions shown in Fig. 8(a), and can be overcome by using the recently demonstrated alternate approaches [43].

To study the performance of the HBR-based decoder, both the codes generated by the encoder were amplified by erbium-doped fiber amplifier, multiplexed by a $2 \times 1$ passive combiner, and then sent into the HBR-based decoder while monitoring both decoder outputs using the optical sampling oscilloscope. Fig. 9(a) shows the autocorrelation signal (the highest peak) representing the decoded code (1, 2, 3). The three smaller peaks represent the MAI due to the cross-correlation signal of code (1, 3, 5). Similarly, Fig. 9(b) shows the autocorrelation signal representing the decoded code (1, 3, 5) and MAI from code (1, 2, 3). The measured bit error rate (BER) for both the codes was $10^{-10}$ when the received signal power is around $-19$ dBm and showed no sign of error floor. The OCDMA system, which generated the same codes with TFF-based coders, reached the same BER at about $-21$ dBm [12]. The experimental results clearly demonstrate the capability of HBR-based devices for multicode processing and, most importantly, showed that an HBR-based system can have similar performances as other systems with different types of coders.

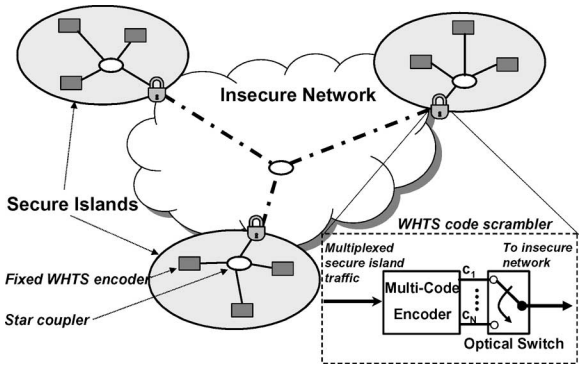


Fig. 10. Schematic of a shared code scrambling network. Nodes are represented by the shaded rectangles and the lock represents the shared code scrambler. The inset shows the architecture of the WHTS code scrambler.

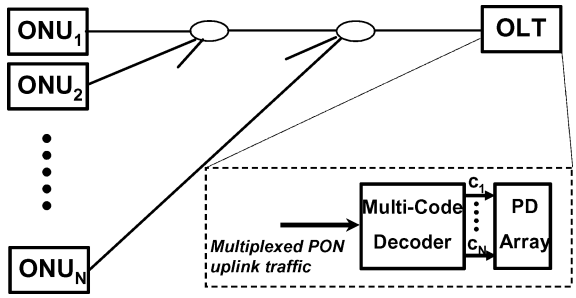


Fig. 11. Schematic of a WHTS OCDMA PON uplink with a multicode decoder configuration at OLT.

The HBR-based en/decoder shows a slight polarization dependency in the form of a slight blue shift of 100 pm for TE-polarized input light. Techniques to reduce this polarization-dependant spectral shift are discussed elsewhere [45]. Additionally, a polarization-dependent loss (PDL) is observed for TE input and is attributed to the apodization-induced out-coupling loss, which is polarization dependent. In our experiments, the polarization of both the codes at the decoder input was adjusted to produce sufficient contrast between the correlation peak and the cross-correlation signal. Alternate apodization approaches with polarization- dependent loss of only 0.2 dB [43] can be used for reduction of the polarization-dependant behavior of the HBR-based devices.

The present encoder/decoder format supports about 20 different 100-GHz-wavelength chips and about five 73.1-ps-time chips. The integrated format is flexible such that larger devices can provide further delays (up to wafer scale trip times) and variable spectral channel width from a few gigahertz to tens of nanometers. Further development will be required to identify firm limits on performance in terms of code count and code design.

## V. Applications of Multicode Processing

In Section IV, we showed the capability of a single HBR-based device for simultaneous multicode processing in WHTS networks. While this development is interesting in itself as a technological breakthrough, simultaneous multicode-processing capability also makes feasible a number of new ideas that can significantly enhance OCDMA network performance. In this section, we summarize some of these ideas that are generally applicable to all types of OCDMA, and not only to WHTS.

### *A. Shared Code Scrambling*

Shared code scrambling was recently proposed [18] in the context of spectral-phase OCDMA to utilize the large phase space for providing enhanced security. A schematic of this idea is shown in Fig. 10, and is applicable to a network scenario where the total network is subdivided into various "secure islands." A secure island is a group of multiplexed users among whom data in the optical domain is deemed secure, and outside of which data in the optical domain is considered insecure. In the proposal of shared code scrambling, a coder was used for each secure island to dynamically scramble the multiplexed traffic of the secure island before transmission into the insecure network. The shared code was unscrambled at the destination to obtain the multiplexed data traffic again. A key was shared among all secure islands to determine the dynamic scrambling sequence. While dynamic scrambling of the assigned code for a single user using on/off keying (OOK) modulation is susceptible to simple energy detection eavesdropping [46], dynamic scrambling of shared code still enhances security (assuming more than one user per secure island). Though proposed initially in the context of spectral phase codes, shared code scrambling can also be generalized to cases when the scrambling mechanism is different (e.g., WHTS) from the coding mechanism used for multiplexing (e.g., spectral phase OCDMA) in the secure islands. The only constraint is that the scrambling process should be reversible to allow the retrieval of the multiplexed data traffic.

While the use of rapidly tunable en/decoders could be used for dynamic shared code scrambling, a multicode ($M$ codes) encoder and optical switch can also be used to dynamically scramble among the $M$ codes. Fig. 10 inset shows this implementation. The size of the multicode encoder and the switching speed is dependant on the security demanded of this scheme. In general, higher number of scrambling codes and higher switching (scrambling) speeds can provide greater security. An analysis of the security provided can be understood only after making exact assumptions of the threat model posed by the eavesdropper (Eve's technology for eavesdropping, network access point, etc.) and the details of the scrambling mechanism implemented. Such an analysis is beyond the scope of this paper and is covered elsewhere [46].

### *B. Passive Optical Network Applications*

While the previous application was based on the use of multicode encoding capability, here we look at how multicode decoding capability can be used for design improvement in a passive optical network (PON) application. Fig. 11 shows the general schematic of a PON, where the optical line terminal (OLT) has to adhere to the uplink data from multiple optical network units (ONU). While current PON implementations use time-domain approaches, WHTS OCDMA PONs have the advantage of asynchronous access and scalability to higher unshared data rates. A single multicode decoder with an array of photodetectors

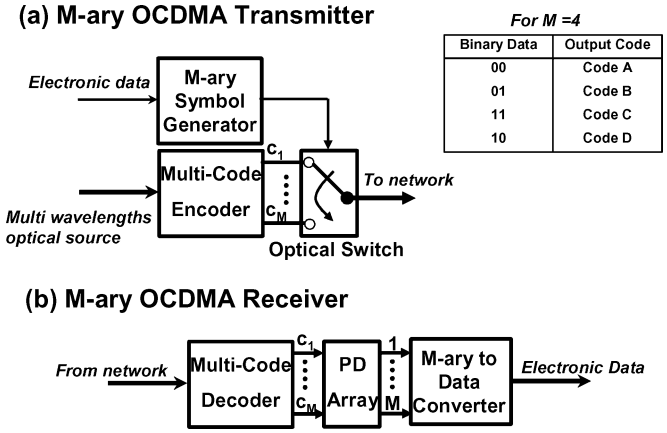


Fig. 12. Implementation of M-ary OCDMA (a) transmitter and (b) receiver.

(shown in the inset of Fig. 11) can be used at the OLT for simultaneous reception of uplink traffic from all ONUs resulting in a much simpler design and lower cost.

### C. Network Monitoring

For practical WHTS network implementations, network monitoring is essential for ensuring that all the user signals are available. The same configuration of the single multicode decoder with a photodetector array can be used by the central network controller to monitor the health of all individual OCDMA signals using a tap off the broadcast star coupler.

### D. Enhanced Scalability Using M-ary Approach

A novel, $M$-ary approach was recently proposed [47] for obtaining high spectral efficiency and network performance in OCDMA networks. In this case, the user is allowed a set of $M$ codes, where each of the $M$ codes will represent a symbol that has a bit length of $\log_2 M$ in binary data. A table for code representation is shown in the inset of Fig. 12(a) for $M = 4$. Our proposal, allowed a tradeoff between spectral efficiency and number of network users by utilizing "wasted code cardinality" for improved network performance. In addition, $M$-ary schemes also thwart simple energy-detection eavesdropping, as an "on" code is sent into the network for all data symbols.

Practical implementation of the $M$-ary approach was limited due to the requirement of $M$ en/decoders at each network node. A recent demonstration used a variation of the $M$-ary approach using pulse-position modulation (PPM) to avoid the requirement for multiple en/decoders, but still required multiple time-gating elements at the receiver for MAI reduction [5].

Multicode en/decoders can be utilized along with a fast optical switch to implement $M$-ary transmitter and receiver as shown in Fig. 12. Unlike in shared code scrambling, the switching speed for the $M$-to-1 optical switch here is decided by the frame rate of code transmission $B/\log_2 M$, where $B$ is the transmission data rate and $M$ is the total number of available symbols or codes. High-speed switches such as lithium niobate electrooptic switches and semiconductor optical amplifier (SOA)-based optical switches have been demonstrated [48]. These switches,

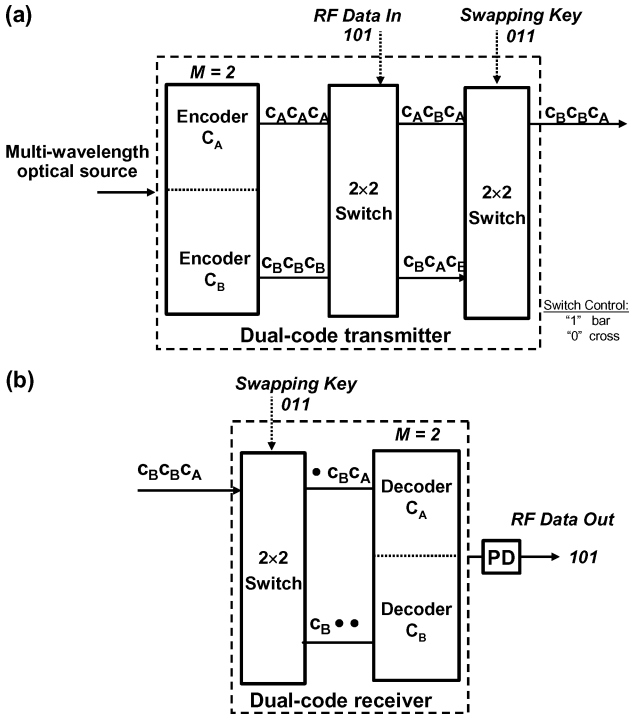


Fig. 13. Schematic of (a) dual-code transmitter and (b) receiver.

TABLE I
OPTICAL OUTPUT AS THE RESULT OF XOR OPERATION

| RF Data | Swapping Pattern | Output Code |
|---|---|---|
| 0 | 0 | Code A |
| 0 | 1 | Code B |
| 1 | 0 | Code B |
| 1 | 1 | Code A |

together with the use of multicode en/decoders, will allow scaling of high speed and large alphabet $M$-ary (e.g., $M = 8$ or 16) OCDMA transmitters and receivers. It should be noted that finite rising and falling edges of the switch will result in some of the chips in a code period being lost, causing a reduction in the code length.

### E. Dynamic M-ary Coding

The ideas of $M$-ary modulation and dynamic code scrambling can be combined to further enhance channel isolation and security. A recent demonstration [12] showed the capability of this scheme for the case of $M = 2$. Fig. 13 shows the implementation of this scheme. The cascade of two $2 \times 2$ switches provides an optical XOR capability, as shown in Table I, to select either of the two codes $C_A$ and $C_B$, to represent and carry bit "1"s and bit "0"s. This code-swapping approach can, thus, provide encryption levels equivalent to the perfectly secure "one-time pads" [49]. The swapping key is assumed to be a pure random sequence, which is unknown to the eavesdropper. This can be ensured in practice by using either a separate secure link such as in quantum key distribution (QKD) [50], or steganographic schemes over public channels [51]. Once again, as shown in Fig. 13, multicode en/decoding can be used to simplify the node architectures.

## VI. Conclusion

In summary, we have looked at the potential of various technology platforms such as TFFs, FBGs, and AWGs to provide a feasible, low-cost path to system implementation of WHTS OCDMA networks. We summarized developments in a relatively new technology based on HBRs that combine the merits of other technology platforms with precise spectral control, compatibility with planar lightwave circuits, and low device footprints. We also presented the experimental results, which demonstrated its capability for simultaneous processing of multiple WHTS codes in a single device.

We also presented a summary of applications where multicode-processing abilities will provide a significant improvement in network performance such as security and scalability. While all these applications can be implemented using an array of devices, a multicode-processing device allows considerable simplification of the node architectures in these applications providing a feasibility path to near-term implementations that are robust, low cost, and light weight. Specifically to WHTS networks, the multicode processing of HBR-based devices with the innate advantages of WHTS such as phase insensitivity and asynchronous access forms an attractive platform for both commercial and military network environments in the near future.

## Acknowledgment

The authors would like to acknowledge helpful discussions with Dr. B. L. Uhlhorn at Lockheed Martin and Dr. E. Narimanov at Princeton University.

## References

[1] A. J. Mendez, R. M. Gagliardi, H. X. C. Feng, J. P. Heritage, and J. M. Morookian, "Strategies for realizing optical CDMA for dense, high-speed, long span, optical network applications," *J. Lightw. Technol.*, vol. 18, no. 12, pp. 1685–1696, Dec. 2000.

[2] K. I. Kitayama, X. Wang, and N. Wada, "OCDMA over WDM PON—Solution path to gigabit-symmetric FTTH," *J. Lightw. Technol.*, vol. 24, no. 4, pp. 1654–1662, Apr. 2006.

[3] L. Tanceski and I. Andonovic, "Wavelength hopping/time spreading code division multiple access systems," *Electron. Lett.*, vol. 30, no. 9, pp. 721–723, 1994.

[4] V. Baby, I. Glesk, R. J. Runser, and R. Fischer *et al.*, "Experimental demonstration and scalability analysis of a four-node 102-Gchip/s fast frequency-hopping time-spreading optical CDMA network," *IEEE Photon. Technol. Lett.*, vol. 17, no. 1, pp. 253–255, Jan. 2005.

[5] C.-S. Bres, I. Glesk, and P. R. Prucnal, "Demonstration of an eight-user 115-Gchip/s incoherent OCDMA system using supercontinuum generation and optical time gating," *IEEE Photon. Technol. Lett.*, vol. 18, no. 7, pp. 889–891, Apr. 2006.

[6] G.-C. Yang and W. C. Kwong, *Prime Codes with Applications to CDMA Optical and Wireless Networks*. Boston: Artech House, 2002.

[7] V. Baby, C.-S. Bres, L. Xu, I. Glesk, and P. R. Prucnal, "Demonstration of differentiated service provisioning with 4-node 253 Gchip/s fast frequency-hopping time-spreading OCDMA," *Electron. Lett.*, vol. 40, no. 12, pp. 755–756, 2004.

[8] W. C. Kwong and G.-C. Yang, "Multiple-length multiple-wavelength optical orthogonal codes for optical CDMA systems supporting multirate multimedia services," *IEEE J. Sel. Areas Commun.*, vol. 22, no. 9, pp. 1640–1647, Nov. 2004.

[9] A. Stok and E. H. Sargent, "Lighting the local area: Optical code division multiple access and quality of service provisioning," *IEEE Netw.*, vol. 14, no. 6, pp. 42–46, Nov./Dec. 2000.

[10] E. S. Shivaleela, K. N. Sivarajan, and A. Selvarajan, "Design of a new family of two-dimensional codes for fiber-optic CDMA networks," *J. Lightw. Technol.*, vol. 16, no. 4, pp. 501–508, Apr. 1998.

[11] C.-S. Bres, I. Glesk, R. J. Runser, and P. R. Prucnal, "All-optical OCDMA code-drop unit for transparent ring networks," *IEEE Photon. Technol. Lett.*, vol. 17, no. 5, pp. 1088–1090, May 2005.

[12] I. Glesk, Y.-K. Huang, C.-S. Brès, and P. R. Prucnal, "OCDMA platform for avionics applications," *Electron. Lett.*, vol. 42, no. 19, pp. 1115–1116, Sep. 2006.

[13] V. Baby, L. R. Chen, S. Doucet, and S. LaRochelle, "Continuous-wave operation of semiconductor optical amplifier-based multi-wavelength tunable fiber lasers with 25GHz spacing," *IEEE J. Sel. Topics Quantum Electron.*, Nov. 2006, to be published.

[14] S. Yegnanarayanan, A. S. Bushan, and B. Jalali, "Fast wavelength-hopping time-spreading encoding/decoding for optical CDMA," *IEEE Photon. Technol. Lett.*, vol. 12, no. 5, pp. 573–575, May 2000.

[15] L. Adam, E. Simova, and M. Kavehrad, "Experimental optical CDMA system based on spectral amplitude encoding of non-coherent broadband sources," *Proc. SPIE.*, vol. 2614, pp. 122–132, 1995.

[16] K.-L. Deng, I. Glesk, K. I. Kang, and P. R. Prucnal, "A 1024-channel fast tunable delay line for ultrafast all-optical TDM networks," *IEEE Photon. Technol. Lett.*, vol. 9, no. 11, pp. 1496–1498, Nov. 1997.

[17] V. Baby, R. J. Runser, I. Glesk, and P. R. Prucnal, "Analysis of a rapidly reconfigurable multicast capable photonic switched interconnect," *Opt. Commun.*, vol. 253, no. 1–3, pp. 76–86, 2005.

[18] R. C. Menendez, P. Toliver, and S. Galli *et al.*, "Network applications of cascaded passive code translation for WDM-compatible spectrally phase-encoded optical CDMA," *J. Lightw. Technol.*, vol. 23, no. 10, pp. 3219–3231, Oct. 2005.

[19] Z. Knittl, *Optics of Thin Films*. New York: Wiley, 1976.

[20] M. Lequime, R. Parmentier, F. Lemarchand, and C. Amra, "Toward tunable thin-film filters for wavelength division multiplexing applications," *Appl. Opt.*, vol. 41, no. 16, pp. 3277–3284, 2002.

[21] H. K. Tsang, M. W. K. Mak, L. Y. Chan, J. B. D. Soole, C. Youtsey, and I. Adesida, "Etched cavity InGaAsP/InP waveguide Fabry-Perot filter tunable by current injection," *J. Lightw. Technol.*, vol. 17, no. 10, pp. 1890–1895, 1999.

[22] R. Parmentier, F. Lemarchand, and M. Cathelinaud *et al.*, "Piezoelectric tantalum pentoxide studied for optical tunable applications," *Appl. Opt.*, vol. 41, no. 16, pp. 3270–3276, 2002.

[23] M. Iodice, G. Cocorullo, F. G. Della Corte, and I. Rendina, "Silicon Fabry-Perot filter for WDM systems channels monitoring," *Opt. Commun.*, vol. 183, no. 5–6, p. 415, 2000.

[24] L. H. Domash, "Thin-films sing a new tune," *Photon. Spectra*, pp. 70–74, Nov. 2004.

[25] S. Sumriddetchkajorn and K. Chaitavon, "A reconfigurable thin-film filter-based $2 \times 2$ add–drop fiber-optic switch structure," *IEEE Photon. Technol. Lett.*, vol. 15, no. 7, pp. 930–932, Jul. 2003.

[26] K. O. Hill and G. Meltz, "Fiber Bragg grating technology fundamentals and overview," *IEEE J. Lightw. Technol.*, vol. 15, no. 8, pp. 1263–1276, Aug. 1997.

[27] R. Kashyap, *Fiber Bragg Gratings*. San Diego: Academic Press, 1999.

[28] J. Magné, D.-P. Wei, S. Ayotte, L. A. Rusch, and S. LaRochelle, "Experimental demonstration of frequency-encoded optical CDMA using superimposed fiber Bragg gratings," in *Proc. Conf. Bragg Gratings, Poling, Photosensitivity Glass Waveguides*, 2003, pp. 294–296.

[29] A. Grunnet- Jepsen, A. E. Johnson, E. S. Maniloff, T. W. Mossberg, M. J. Munroe, and J. N. Sweetser, "Demonstration of all-fiber sparse lightwave CDMA based on temporal phase encoding," *IEEE Photon. Technol. Lett.*, vol. 11, no. 10, pp. 1283–1285, Oct. 1999.

[30] J. H. Lee, P. C. The, P. Petropoulos, M. Ibsen, and D. J. Richardson, "A grating-based OCDMA coding-decoding system incorporating a nonlinear optical loop mirror for improved code recognition and noise reduction," *IEEE J. Lightw. Technol.*, vol. 20, no. 1, pp. 36–46, Jan. 2002.

[31] S. Kutsuzawa, N. Minato, S. Oshiba, A. Nishiki, and K. Kitayama, "10 Gb/s $\times$ 2 ch signal unrepeated transmission over 100 km of data rate enhanced time-spread/wavelength-hopping OCDMA using 2.5Gb/s-FBG en/decoder," *IEEE Photon. Technol. Lett.*, vol. 15, no. 2, pp. 317–319, Feb. 2003.

[32] L. R. Chen, "Flexible fiber Bragg grating encoder/decoder for hybrid wavelength-time optical CDMA," *IEEE Photon. Technol. Lett.*, vol. 13, no. 11, pp. 1233–1235, Nov. 2001.

[33] L. R. Chen, P. W. E. Smith, and C. M. de Sterke, "Wavelength-encoding/temporal-spreading optical code-division multiple access system with in-fiber chirped Moire gratings," *Appl. Opt.*, vol. 38, no. 21, pp. 4500–4508, 1999.

[34] G. P. Agrawal, *Fiber-Optic Communication Systems*, 3rd ed. New York: Wiley Inter-Science, 2002.

[35] R. Ramaswami and K. N. Sivarajan, *Optical Networks—A Practical Perspective*, 2nd ed. San Mateo, CA: Morgan Kaufman, 2002.
[36] M. Koga, Y. Hamazumi, and A. Watanabe *et al*., "Design and performance of an optical path cross-connect system based on wavelength path concept," *J. Lightw. Technol*., vol. 14, no. 6, pp. 1106–1119, Jun. 1996.
[37] M. C. Nuss, W. H. Knox, and U. Koren, "Scalable 32 channel chirped-pulse WDM source," *Electron. Lett*., vol. 32, no. 14, pp. 1311–1312, 1996.
[38] A. Bellemare, M. Karasek, M. Rochette, S. LaRochelle, and M. Tetu, "Room temperature multifrequency erbium-doped fiber lasers anchored on the ITU frequency grid," *J. Lightw. Technol*., vol. 18, no. 6, pp. 825–831, Jun. 2000.
[39] S. Chandrasekhar, M. Zirnbigl, A. G. Dentai, C. H. Joyner, F. Storz, C. A. Burrus, and L. M. Lunardi, "Monolithic eight-wavelength demultiplexed receiver for dense WDM applications," *IEEE Photon. Technol. Lett*., vol. 7, no. 11, pp. 1342–1344, Nov. 1995.
[40] Z. J. Sun, K. A. NcGreer, and J. N. Broughton, "Demultiplexer with 120 channels and 0.29 nm channel spacing," *IEEE Photon. Technol. Lett*., vol. 10, no. 1, pp. 90–92, Jan. 1998.
[41] K. Yu, J. Shin, and N. Park, "Wavelength-time spreading optical CDMA system using wavelength multiplexers and mirrored fiber delay lines," *IEEE Photon. Technol. Lett*., vol. 12, no. 9, pp. 1278–1280, Sep. 2000.
[42] G. Cincotti, N. Wada, and K. I. Kitayama, "Characterization of a full encoder/decoder in the AWG configuration for code-based photonic routers—Part I: Modeling and design," *J. Lightw. Technol*., vol. 24, no. 1, pp. 103–112, Jan. 2006.
[43] D. Iazikov, C. M. Greiner, and T. W. Mossberg, "Integrated holographic filters for flat-passband optical multiplexers," *Opt. Express*, vol. 14, p. 3497, 2006.
[44] Y.-K. Huang, V. Baby, P. R. Prucnal, C. M. Greiner, D. Iazikov, and T. W. Mossberg, "Integrated holographic encoder for wavelength-hopping/time-spreading optical CDMA," *IEEE Photon. Technol. Lett*., vol. 17, no. 4, pp. 825–827, Apr. 2005.
[45] C. M. Greiner, D. Iazikov, and T. W. Mossberg, "Low-loss silica-on-silicon two-dimensional Fabry-Perot cavity based on holographic Bragg reflectors," *Opt. Lett*., vol. 30, no. 1, pp. 38–40, 2005.
[46] T. Shake, "Security performance of optical CDMA against eavesdropping," *J. Lightw. Technol*., vol. 23, no. 2, pp. 655–670, Feb. 2005.
[47] E. Narimanov, W. C. Kwong, G.-C. Yang, and P. R. Prucnal, "Shifted carrier-hopping prime codes for multicode keying in wavelength-time O-CDMA," *IEEE Trans. Commun*., vol. 53, no. 12, pp. 2150–2156, Dec. 2005.
[48] T. S. El Bawab, *Optical Switching*. New York: Springer, 2006.
[49] C. E. Shannon, "Communication theory of secrecy system," *AT&T Tech. J*., vol. 28, pp. 656–715, 1949.
[50] P. Toliver, R. J. Runser, and T. E. Chapuran *et al*., "Experimental investigation of quantum key distribution through transparent optical switch elements," *IEEE Photon. Technol. Lett*., vol. 15, no. 11, pp. 1669–1671, Nov. 2003.
[51] B. B. Wu and E. E. Narimanov, "A method of secure communications over a public fiber-optical network," *Opt. Express*, vol. 14, no. 9, pp. 3738–3751, May 1, 2006.

**Yue-Kai Huang** (S'04) received the B.S. degree in electrical engineering and the M.S. degree in electrooptical engineering from National Taiwan University, Taipei, Taiwan, in 2000 and 2002, respectively. He is currently working toward the Ph.D. degree in electrical engineering at Princeton University, Princeton, NJ.

Since 2004, he has been with the Lightwave Communication Research Laboratory, Princeton University. His current research interests include designing OCDMA code-processing devices, security study on OCDMA networks, ultrafast SOA switching applications, and all-optical regeneration system.

**Varghese Baby** (S'00) was bom in Trivandrum, Kerala, India, in 1978. He received the B.E. degree in electrical engineering from the Indian Institute of Technology Madras, Chennai, India, in 2000 and the M.S and Ph.D. degrees in electrical engineering from Princeton University, Princeton, NJ, in 2002 and 2006, respectively.

Since January 2006, he has been a Postdoctoral Research Fellow in the Photonics Systems Group at McGill University, Montreal, PQ, Canada. His current research interests include fiber lasers, fiber-optic sensors, and all-optical networking.

**Ivan Glesk** (M'01–SM'01) received the the D.Sc. degree from Slovak Academy of Sciences, Bratislava, Slovak Republic, and the Ph.D. degree in quantum electronics and optics from Comenius University, Bratislava.

He joined Comenius University in 1986, where he became a Professor of physics in the Department of Experimental Physics. He joined the Department of Electrical Engineering, Princeton University, Princeton, NJ, in 1991, where he is currently a Senior Research Scholar. He is also a Manager of the Lightwave Communication Research Laboratory, Princeton University. He has Coauthored 16 book chapters and over 200 publications. He has presented 18 invited talks at various international conferences and holds three U.S. patents. His current research interests include ultrashort pulsed laser, data processing, and optical networks and interconnects.

Prof. Glesk is a recipient of the International Research and Exchange Board Fellowship.

**Camille-Sophie Bres** (S'04) was born in Montpellier, France. She received the B.S. degree(honors) in electrical engineering from McGill University, Montreal, QC, Canada, in 2002 and the M.S. and Ph.D. degrees in electrical engineering from Princeton University, Princeton, NJ, in 2004 and 2006, respectively.

Her research interests include all-optical networks, system design, and optical CDMA.

**Christoph M. Greiner** (M'02) received the M.A. and Ph.D. degrees in optical physics from the University of Oregon, Eugene, in 1995 and 2002, respectively.

Since 2002, he has been a Senior Scientist with LightSmyth Technologies, Eugene, OR. His current research interests include development of integrated photonic components based on planar holographic Bragg reflectors.

Dr. Greiner is a member of the American Physical Society, the German Physical Society, the Optical Society of America, and the International Society for Optical Engineers.

**Dmitri Iazikov** (M'03) was born in St. Petersburg, Russia, in 1971. He received the B.S. and M.S. degrees in applied optics from Moscow University of Physics and Technology, Moscow, Russia, in 1990 and 1993, respectively.

He has recently held positions as Design Authority at JDS Uniphase Corporation, San Jose, CA, in thin-film-filter-based wide-band wavelength-division-multiplexing group and as Technical Lead for arrayed-waveguide grating and optical add–drop multiplexing development at Zenastra Photonics, Ottawa, ON, Canada. Since 2002, he is a Senior Scientist with LightSmyth Technologies, Eugene, OR. His current research interests include design and characterization of holographic-Bragg-reflector-enabled planar lightwave circuits.

**Thomas W. Mossberg** (M'96) received the B.A. degree from the University of Chicago, Chicago, IL, in 1973 and the M.A. and Ph.D. degrees from Columbia University, New York, in 1975 and 1978, respectively.

He has been on the faculties of Columbia University, Harvard University, and the University of Oregon. He cofounded Templex Technology, Inc., Eugene, OR, in mid-90s. He is currently the Chief Technology Officer of LightSmyth Technologies, Eugene, specializing in the design and fabrication of planar holographic optical devices and distributed photonic circuits. He has authored approximately 140 refereed papers in several technical journals.

Dr. Mossberg is a Fellow of the American Physical Society and the Optical Society of America.

**Paul R. Prucnal** (S'75–M'78–SM'90–F'92) received the A.B. degree from Bowdoin College, Brunswick, ME, in 1974 and the M.S., M. Phil., and Ph. D. degrees from Columbia University, New York, in 1976, 1978, and 1979, respectively.

Since 1988, he is a Professor of electrical engineering with Princeton University, Princeton, NJ, where he was an Acting Director of the Center for Photonics and Optoelectronics Materials from 1990 to 1992. He has Authored over 100 publications and holds five patents. His research interests include experimental and theoretical work on optical multiple-access techniques for broadband networks, photonic fast packet switching with optically processed control, and optical multiprocessor interconnects.

Prof. Prucnal is currently an Associate Editor for the IEEE TRANSACTIONS ON COMMUNICATIONS in the area of optical networks. He is on the Editorial Board for *Optical Fiber Technology* and the Advisory Board for *Photonic Network Communications*. Since 1997, he has been a Fellow of the Optical Society of America. He is a recipient of the 1990 Rudolf Kingslake Medal from the International Society of Optical Engineering.